Three-Dimensional Display in Nuclear Medicine and Radiology

Jerold W. Wallis and Tom R. Miller

Mallinckrodt Institute of Radiology, Washington University School of Medicine, St. Louis, Missouri

As three-dimensional displays become more common in nuclear medicine and radiology, it is important to know when they should be employed. Selection of the appropriate three-dimensional rendering method requires an understanding of the techniques and both their advantages and limitations. This review article is intended to provide an introduction to three-dimensional rendering techniques. Methods in surface mapping, surface rendering, and volume rendering are presented, with discussion of specific clinical applications in nuclear medicine, computed tomography, and magnetic resonance imaging.

J Nucl Med 1991; 32:534–546

Tomographic imaging is widely employed in medical imaging including nuclear medicine, computed tomography (CT), and magnetic resonance imaging (MRI). While tomographic studies are usually interpreted from images presented as series of slices, there is increasing interest in presentation of the data in a more realistic three-dimensional form. These new displays provide an overview of the many slices in a single image, and they enhance the perception of spatial relationships. By providing easily understood, life-like presentations of the image data, three-dimensional displays aid communication between the imaging specialist, who is trained in the interpretation of slice data, and the referring physician who may be uncomfortable in dealing with large numbers of slices.

The obvious and important question of diagnostic accuracy arises when considering three-dimensional displays. At this time there are no convincing studies of this issue in nuclear medicine (with the exception of bull's-eye displays in thallium scintigraphy), and careful evaluation has been performed in only a few CT studies. Studies using CT have demonstrated that three-dimensional displays can either clarify or obscure diagnostic information, depending on the clinical application and the type of display. Therefore, examinations employing three-dimensional displays should be interpreted with caution and in conjunction with the slice data.

Most "three-dimensional displays" are actually two-dimensional pictures that can be displayed on computer screens. These pictures contain depth cues that allow us to interpret the image contents as three-dimensional objects. The term "rendering" is employed for the process of converting the three-dimensional image data into a viewable form; typically, the rendered images represent condensed versions of the original data. Several forms of three-dimensional rendering are available, and an appropriate technique must be chosen to preserve the diagnostic information in the final image.

With the increasing availability of powerful computers and the proliferation of single-photon emission computed-tomography (SPECT) and positron emission tomography (PET), this is a favorable time for further development of three-dimensional techniques in nuclear medicine. In this paper, current display methods will be reviewed with emphasis on work in nuclear medicine.

METHODS

Display Techniques

Many types of three-dimensional displays have been developed; the most common forms are listed in Table 1 and discussed below.

Slice Display. The simplest and most common three-dimensional technique is display of multiple transverse slices, perhaps with the presentation of sagittal and coronal slices as well. This form of display has the advantage that all of the data are present in unmodified form, but great demands are placed on the viewer for integration of the image information.

Two-dimensional Mapping. When the data approximate a curved surface, a direct mapping can be constructed from the curved surface to a flat image, as is done in cartography. This technique has been applied extensively in myocardial imaging where the thin myocardium can be considered to be a surface.

Surface Rendering. Surface rendering is a "binary" operation in which the first step is to examine each

Received Nov. 5, 1990; revision accepted Nov. 5, 1990.
For reprints contact: Jerold W. Wallis, MD, Mallinckrodt Institute of Radiology, 510 South Kingshighway, St. Louis, MO 63110.

TABLE 1
Types of Three-Dimensional Displays

Display type	Subcategories		Major applications
Slice display	Orthogonal slices		Any tomographic imaging
	Oblique slices		Cardiac SPECT, Cardiac MR
Mapping	Bull's-eye		Cardiac SPECT
	Cylindrical display		Cardiac SPECT
Three-dimensional rendering	Surface rendering	Polygon tiling	Computer-aided design (industrial), radiation therapy planning, cardiac SPECT, medical surface modeling
		Binary voxel rendering (cuberille)	Cardiac SPECT, bone CT, brain and heart MR
	Volume rendering	Summed projection	Simulation of planar images from slice data
		Maximum activity projection	Bone, gallium, and blood-pool scintigraphy, MR angiography
		Volumetric compositing	Bone and soft-tissue CT, brain MR, and radiation therapy planning

voxel (i.e., three-dimensional pixel) in the image and decide whether it is inside or outside of the objects being imaged. All other information in the image is typically discarded. Depth cues may then be added as described below; frequently illumination serves as the primary depth cue. Two subcategories of surface rendering exist: the surface can be approximated using many small triangles or rectangles, leading to a wire mesh appearance and referred to as polygon tiling; surface rendering methods that use a uniform matrix of cubic voxels rather than polygon tiling have been called cuberille or binary voxel techniques (*1*). In either case, the resulting image contains only object surfaces. Optionally, functional information may then be mapped onto the surface for display purposes. Care must be taken to distinguish these binary algorithms from volume rendering of surfaces (discussed in the section on volumetric compositing).

The process of dividing an image into its component parts is referred to as image segmentation. Thresholding, gradient-based edge detection, and manual drawing of regions have been employed in segmentation of both two- and three-dimensional images. Image segmentation can be both advantageous and detrimental in three-dimensional display. Image segmentation permits display of object surfaces and facilitates calculation of the volumes of objects in the image, such as cardiac chamber volumes for ejection fraction calculation. However, inaccuracies in the segmentation process, sometimes caused by use of inappropriate thresholds, can cause major errors in the rendered images. Objects near the threshold (such as ribs and other thin objects affected by the partial volume effect) may become discontinuous, leading to creation of artifactual surfaces. The image may contain voxels whose classification is uncertain, either because of blur or partial volume effect, or because the tissues are indistinguishable using a particular imaging modality. Binary segmentation forces voxels into categories, with arbitrary classification of ambiguous voxels; the rendered image no longer conveys the uncertainty present in the image data.

The major advantages of surface rendering are computational efficiency and ease of implementation. In addition, surface rendering is ideal for applications based entirely upon geometry, such as animation or industrial applications employing solid modeling. The greatest disadvantage of this technique in medical imaging is that all information about the interior of objects is discarded. In nuclear medicine, diagnostic information is only infrequently contained along organ surfaces. In addition, inaccuracies in the segmentation process can introduce misleading information into the rendered images.

Volume Rendering. Volume rendering techniques do not employ segmentation as the primary step; instead, image information from the whole volume of data is combined along rays to form a rendered projection image (Fig. 1). Various ways of combining information have been proposed, and each results in a different type of image.

Summing the image data along rays through the three-dimensional data set onto the viewing plane (summed projection) produces images very similar to planar images. This technique has been used in x-ray CT, SPECT (*2, 3*), and tomographic light microscopy (*4*). These images can aid in observer orientation when

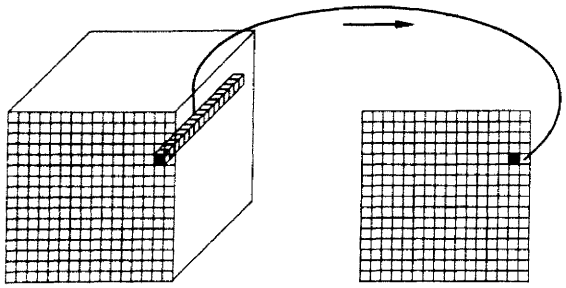

FIGURE 1
Following tomographic reconstruction, transverse slices are stacked to form a cube. Intensity information from voxels along rays passing though the cube are combined and placed in the corresponding pixel in the rendered two-dimensional image.

interpreting the tomographic data, but much of the enhanced contrast gained by use of tomography is lost when summed projection is employed (*5*) (Fig. 2).

Choosing the maximum voxel value along rays (maximum activity projection) rather than the sum of voxel values is appropriate when the most intense objects in the image are the objects of greatest interest in the diagnostic study. As illumination is not employed, other depth cues need to be utilized to convey a three-dimensional effect. Depth weighting can be added using simulated exponential attenuation before finding the maximum voxel, thus leading to the following equation:

$$I_{x,y} = \overset{n}{\underset{z=1}{M}}\, e^{-\mu_r z} D_{x,y,z} \qquad (1)$$

where I is the rendered image, D is the n × n × n cube of data, μ_r is the attenuation coefficient, and M is the maximum operator used to choose the greatest value along the ray undergoing reprojection. Since attenuation is used to enhance the three-dimensional effect, realistic gamma-ray attenuation values need not be used. Typically, attenuation coefficients of 0.024 to 0.049 cm^{-1} are used in nuclear medicine studies.

Rendering the study from 32 to 64 angles about the patient and displaying the rendered images in continuous cine format provides the illusion of rotation, thus allowing the viewer to easily distinguish anterior fro posterior structures. Depth-weighted maximum activit projection has been proposed by us for use in "ho spot" imaging in nuclear medicine (*5–7*), and it ha been used in MRI angiography (*8, 9*). In many scint graphic imaging applications, maximum activity pr jection incorporates the best features of both the slic display and planar images. Object contrast in image produced using maximum activity projection is superior to that observed in summed projection (Fig. 2) and is similar to the high contrast present in tomographic slices (*5*). This display is superior to both planar and slice images in facilitating orientation in three dimensions and aiding in appreciation of structural relationships.

Transparent objects and images of surfaces can be produced by volume rendering using a technique sometimes referred to as "volumetric compositing"; several variations of this algorithm have been developed (*10, 11*). In these techniques, each voxel in the image is assigned a color (C_i) and an opacity (α). The opacity parameter determines how much of the color from voxels in back is transmitted through to the viewer (Fig. 3).

If the voxels are thought of as luminous objects with a color C_i, and colors are accumulated from back to front, the color emitted (C_{out}) from the ith voxel would be:

$$C_{out} = C_i + (1 - \alpha_i)C_{in}. \qquad (2)$$

For example, in a CT image, voxels could be classified based on Hounsfield number, assigning opaque/white to voxels having a bone density, translucent/red to soft tissue, etc. Note that voxels having an intermediate density are assigned intermediate opacities/colors; this assignment method represents a major difference from the binary algorithms described above, leading to reduction of errors due to mis-classification compared to the binary method. Surfaces can be depicted by modifying both opacity and color based on gradients in the image such that only edges will have the highest value permitted to a given tissue, and by using a simulated light source to modulate the intensity of C_i (*10*). For luminous objects (Equation 2), the opacity does not affect the color (C_i) originating in a given voxel. When

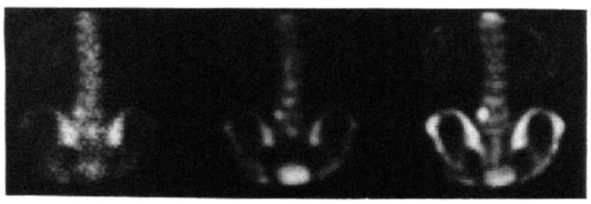

FIGURE 2
Bone scintigraphy in a patient with spondylolisthesis at L5 following trauma: (left) raw projection image from SPECT acquisition; (center) image following reconstruction and summed projection; (right) same image, utilizing maximum activity projection. The lesion is more clearly seen following maximum activity projection that in the other two images.

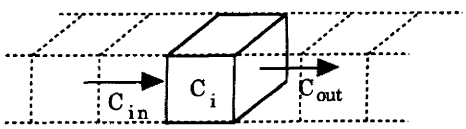

FIGURE 3
Light emitted by voxels at the rear of the image passes into voxel (C_i) and is diminished due to the voxel opacity (α_i); this light then is combined with the light emitted by the voxel (C_i) to form the emitted light (C_{out}). The same process is repeated for each voxel, moving from the back to the front of the image cube.

illumination is used, the opacity should affect C_i, as transparent objects do not reflect light well. Thus, a modified form of the above equation is used when lighting is employed:

$$C_{out} = \alpha_i C_i + (1 - \alpha_i) C_{in}. \quad (3)$$

The main advantages of volumetric compositing are that very life-like renderings can be produced that portray multiple tissue types simultaneously and that image inaccuracies due to minor segmentation errors and aliasing are reduced. Unfortunately, the technique is much more computationally intensive than either the binary algorithms or the simpler projection techniques described above. There are many parameters that must be adjusted in order to optimize the quality of the rendered image. Perhaps most importantly, one must ensure that the features of the original image needed for diagnosis are well portrayed in the rendered image; display of illuminated surfaces is of little use when the diagnostically useful information is manifested as slight variations within organs that are not shown on the rendered images.

Depth Cues. When producing three-dimensional renderings, several forms of depth cues can be added during image generation to give the illusion of a third dimension (Table 2). These depth cues can be applied in various combinations to the rendering techniques described above (e.g., a polygon tiled surface could be produced using hidden surface removal, depth weighting, and illumination as depth cues).

Stereoscopic displays present each eye with a slightly different image; the visual system combines these images and adds the perception of depth. Although in limited use currently, stereoscopic images have been available in conventional chest radiography since 1907 (*12, 13*) and the technique has been available in neuroradiology for three decades (*14–16*). Applications in nuclear medicine have also been explored (*3, 17*). Recent advances in liquid crystal technology and polarized displays facilitate viewing of stereoscopic images from digital workstations.

Hidden surface removal refers to the erasure of portions of surfaces from the image when they are behind other objects. This technique attempts to model one aspect of everyday viewing of real objects. While hidden surface removal appears simple, two crucial questions must be addressed: (1) What are the objects and their associated surfaces in the image, and how can they be defined? (2) Are objects completely opaque, or are they translucent (e.g., multicolored jello)?

When depth coding or distance weighting is applied, distant objects become fainter or less intense than closer objects. This phenomenon is similar to the attenuation present in planar scintigraphy; for example, posterior rib lesions are easily distinguished from anterior ones in bone scintigraphy because of attenuation. Early applications of three-dimensional surface display in radiology utilized depth weighting and hidden object removal as the only depth cues. As is evident in Figure 4 (left), most fine surface detail is lost with this technique because slight variations in depth from irregularities on object surfaces are small in comparison to the total anterior-posterior extent of the image.

Subsequent work in three-dimensional display utilized illumination to accentuate surface detail (*18*). When illuminated from the side, variations in a surface produce a pattern of shadows and highlights in the image (Fig. 4 right), which we interpret to be changes in surface contour based on our experience with real objects. The process of simulated illumination is shown in Fig. 5.

Simulated rotation through use of cine loops provides an even greater three-dimensional effect. Additionally, rotation allows interpretation from multiple angles, frequently revealing details that were hidden on a single projection. If rotation is utilized and objects are not opaque, depth weighting must also be employed to avoid visual confusion regarding the direction of rotation (*19*). The viewing plane can be rotated either by tracing rays obliquely through the cube of data or by rotating the entire cube and then tracing along columns.

TABLE 2
Types of Depth Cues

Stereoscopic display
Hidden line/surface removal
Depth weighting
Illumination
Rotation

Data Representation

Wire Frame/Polygon. Much of the early work in segmentation rendering of medical images involved conversion of the edge information to a wire frame surface composed of multiple polygons. These polygons then can be shaded using standard illumination algorithms (*18*). This type of three-dimensional representation is still used extensively for other applications in computer graphics, and image workstations are fre-

FIGURE 4
Surface rendering of the skull of a normal child, derived from CT data. The effect of different depth cues: (left) depth weighting only; (right) illumination and depth weighting. (Illustration courtesy of M. Vannier, MD.)

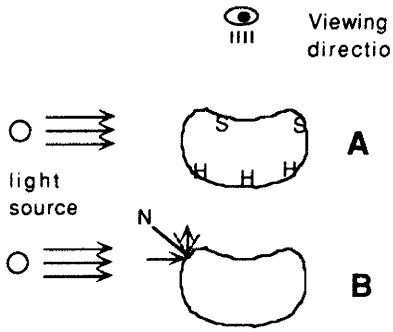

FIGURE 5
Simulated illumination: After selection of a viewing direction and a light source position, portions of the object can be designated as being hidden from view (H) or in complete shadow (S). For the remaining portions of the object, normals (N) perpendicular to the object are computed (B). These normal vectors can be generated from gradients in the original data set or from the contours of the detected edges. Incident light (arrows) preferentially bounces off the object at an angle with respect to the surface normal. Lesser amounts of light reflect at other angles (shorter dotted lines) depending on the characteristics assigned to the surface. If desired, a component of diffuse lighting can be added to partially illuminate those portions of the object in complete shadow. Unless stereoscopic images are being generated, a viewing plane (parallel rays) is usually used rather than a viewing point (perspective viewing).

quently rated by the number of polygons/second that can be shaded and displayed.

Z-buffer. Rather than converting from voxel edges to polygons, the data can be left in voxel form, recording only the depth into the cube of edge voxels belonging to the object at each point. Gradients can then be computed from the depth or "Z-buffer" information alone, by examining a 3 × 3 neighborhood around each point to determine surface direction (*20*). This method is quite fast, but results in coarser illumination than other methods because the number of possible surface directions is limited by the size of the voxels. Inaccuracies may also result at edges of overlapping structures.

Octree. An alternate compact method of storing edge information is in an octree (*21*). The cube containing the segmented objects can be divided into octants (three-dimensional quadrants). If the contents of an octant is nonuniform, it is subdivided further; if it is uniform (either object or background), it is given the corresponding value and not further divided. This method permits rapid traversal through the data when performing rendering. Similar to the methods above, only edge information is retained in this representation.

Cube of Voxels. Slices are the most basic form of data representation for tomographic data. These slices can be stacked together in the computer to form a cube. The volume rendering algorithms require that the image data remain in this format so that all grey scale information is available during the image rendering process.

When tomographic slices are acquired, the inter-slice spacing is not always the same as the pixel size within slices; this results in voxels that are rectangular solids rather than cubes. For purposes of ray tracing, illumination, and rotation, it is more convenient to first interpolate the data so that voxels have the same size in all dimensions. Most commonly, linear or trilinear interpolation is utilized. Other alternatives include nearest neighbor interpolation (which yields a coarser image) and frequency domain interpolation (which is more computationally expensive). When interpolation is performed on images that have already been segmented into objects and edges, it is possible to perform shape-based interpolation (*22*) to connect edges in the image.

When axial sampling is relatively coarse, an additional consideration arises—the partial volume effect arising from under-sampling. For example, in positron tomography the heart may be encompassed by as few as four or five widely spaced slices. Thus, there is a danger of axial undersampling leading to potentially significant artifacts caused by aliasing. Recent analyses indicate that slice spacing should not be greater than one-half the resolution expressed as the axial full-width at half-maximum (*23*). For typical PET tomographs, this leads to the requirement for at least 14 slices over 80–100 mm. If cardiac image data are collected without electrocardiographic gating, as is usually the case, the motion blurring will worsen the effective axial resolution, thus relaxing the sampling requirement. Visually satisfactory results with ungated images of the heart have been obtained with a 7-slice tomograph (*24*).

Computer and Display Requirements

Three-dimensional display places heavy demands on storage, processing, and display equipment. A typical SPECT study is acquired as a series of 64 transaxial slices each with a 64 × 64 pixel matrix of two-byte words. Thus, one-half megabyte of disk storage is required. If 128 × 128 images are required, the complete image cube will be eight times larger, thus using four megabytes of disk space. A gated cardiac blood-pool study will usually consist of 16 time frames generating a total of 4–8 megabytes of data, depending on whether byte mode or word mode is employed. Although these numbers are large, they are within the capabilities of modern magnetic disks, and long-term storage can be accomplished using optical disks or helical 8-mm tape cartridges.

Computer memory is, perhaps, a more critical issue. Most three-dimensional display algorithms deal with the entire cube of image data at one time. Thus, one-half or, preferably, one megabyte of data should be stored in computer memory. The older 16-bit computers that are still widely employed in nuclear medicine cannot effectively access more than one-sixteenth of a megabyte of data, thus hindering implementation of the newer display algorithms. For this reason, more

than because of differences in speed, the newer 32-bit machines are important to the application of modern three-dimensional display methods. With careful programming, three-dimensional reconstruction has also been implemented on IBM PC/AT class machines (*25*).

Rotation of three-dimensional image cubes and ray tracing are the primary computational algorithms in most three-dimensional display techniques; reconstruction by filtered backprojection and digital filtering are important as precursors to the three-dimensional rendering. Measurements in our laboratory reveal that oblique rotation with interpolation of a 64 × 64 × 64 voxel image cube requires approximately 160 sec on a microVAX II (Digital Equipment Corp., Maynard, MA), a 32-bit computer running at 0.9 MIPS (million instructions per second). Use of an array processor reduces the time to 2–4 sec. Ray tracing requires 4.4 sec on the microVAX II and 0.2 sec on the array processor. Thus, the array processor is an important component of an efficient system for three-dimensional rendering as it is for backprojection reconstruction of SPECT data. In the near future, reduced instruction set (RISC) desktop workstations and RISC math coprocessors should be available that run at speeds of 10–25 MIPS or more. These powerful but low-cost machines with 10–30 times the speed of a microVAX II should reduce the computation times dramatically without the cost and programming inconvenience of the array processor.

The final hardware component of a three-dimensional display system, the video display, is readily available. All modern displays have the capacity to display at least a 512 × 512 pixel image with 256 colors or gray levels. The most demanding aspect of nuclear medicine display is the rapid presentation of images in cine form, with zooming of the (relatively small) images up to full screen size. Paradoxically, older frame buffer systems with hardware support for image zoom and cine display may have some advantages over the newer workstations which have general-purpose display systems and lack these hardware features.

CLINICAL APPLICATIONS IN NUCLEAR MEDICINE

"Hot Spot" Imaging

Bone and gallium scintigraphy, liver blood-pool imaging (for hemangioma detection), and monoclonal antibody studies principally involve detection of "hot spots." These studies have several characteristics in common:

1. There can be wide variation of activity in both normal and abnormal areas.
2. Variations of activity within organs contain diagnostic information and are important to preserve in a rendered image.
3. Surface detail of organs is relatively unimportant, and subtle surface variation is lost due to resolution and noise limitations.
4. The most intense areas of uptake contain the most diagnostic information.

The first two characteristics make it difficult to use thresholding as an effective tool in image segmentation, thus limiting the use of any of the binary surface rendering techniques. The second and third characteristics make surface images inappropriate, whether produced by surface rendering or volume techniques. The last characteristic suggests that when low-activity and high-activity structures overlap in an image, the higher activity structure should be depicted. Thus, volume rendering utilizing maximum-activity projection is likely to be most appropriate for use in these studies (*6*). Summed projection has also been proposed for use in nuclear medicine (*2, 3*), but that technique results in loss of image contrast compared to maximum activity projection (*5*).

Typical bone and blood-pool images produced with depth-weighted maximum activity projection are shown in Figure 6. A cine sequence of volume rendered images can be produced in less than 4 min from the reconstructed slices using either an array processor, workstation, or high-end personal computer. Volume rendering, employed routinely in our clinic for almost two years, has been found to be valuable in the interpretation of clinical SPECT and PET studies.

Cardiac Imaging

Perhaps the most widespread and successful applications of three-dimensional displays have been in cardiac imaging. Three areas will be considered here: myocardial imaging, display of physiologic information (functional imaging), and gated blood-pool studies.

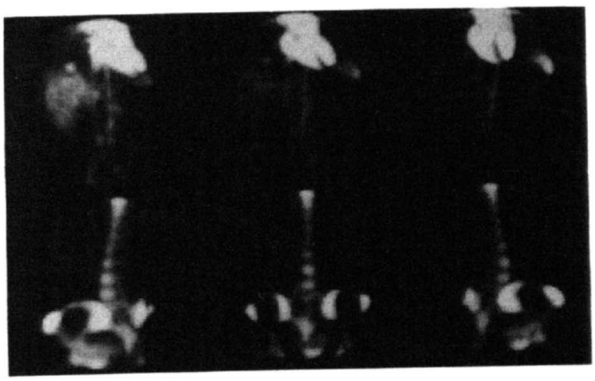

FIGURE 6
Volume rendering in "hot spot" imaging. (Top) hepatic blood-pool study demonstrating a small hemangioma at the dome of the liver. (Bottom) normal bone scintigraphy. Images were produced from several angles using depth-weighted maximum activity projection.

Fundamental to all cardiac display methods is the fact that the heart sits obliquely in the chest. Thus, the conventional slice images generated in transaxial, coronal and sagittal planes are not well suited to the orientation of the heart. Thus, the first step in all three-dimensional displays of the heart is rotation of the image data so the long axis of the left ventricle is along one of the primary axes. The resulting short- and long-axis slices will be oriented in a standardized way with no walls imaged tangentially.

Perfusion Imaging. The polar, or bull's-eye, display has achieved great popularity in thallium-201 myocardial imaging (*26, 27*), and its diagnostic utility has been validated in a multicenter trial (*28*). In this display method, 10 or more short-axis slices are arranged as expanding concentric rings with the apex at the center and the base of the heart at the periphery. The activity in each segment of each ring is determined by a radial search of each short axis slice. In this display, the positions of the myocardial segments will be standardized between patients. Thus, quantification is possible with comparison of normal values between different patients. At least two methods of performing the radial search are in use. The simplest technique involves determination of the most intense pixel along each of 64 radials from the ventricular center for each short-axis slice. In a more complicated but potentially more accurate method, the thickness of the myocardium is taken into account by averaging the activity within a small radial ring for each radial sector (*29*).

The conventional bull's-eye display suffers from uncertainty about the activity at the apex. Since radial searches are performed along each short-axis slice, the exact position and activity of the apex is uncertain because that region is crossed tangentially. Some workers have not attempted to assign an activity value at the apex, while others have interpolated values obtained from a long-axis slice through the apex. More recently a modification of the bull's-eye has been proposed that addresses the apical problem by searching radially in three dimensions rather than in two dimensions along each short-axis slice (*24*). In this method, the entire three-dimensional cube of image data is held in the computer memory. The radial searching is then performed in all directions radially from the ventricular center. Thus, the apex is evaluated with an approximately normally-directed searching vector in the same way as all the other walls (Fig. 7, upper left). An alternative to the full three-dimensional method is to model the left ventricle as a cylinder with a hemispherical cap (*30*). Searching is then performed radially in two dimensions on the short axis slices in the basal and mid-portions of the ventricle and in a three-dimensional way at the apical cap. As an alternate to polar displays, the cardiac perfusion data can be displayed in a cylindrical projection (Fig. 7, lower left) (*24*). This is analogous to the Mercator projection used in cartography, in which the Earth is viewed from the side.

Bull's-eye and cylindrical projections distort the heart just as the polar and Mercator projections distort the Earth. One approach to the problem in the bull's-eye display is to change the area of each concentric short-axis ring as the bull's-eye image is created so the true myocardial areas are retained (*30, 31*). More elaborate techniques employed in map making to reduce the effect of distortion have not been evaluated in nuclear medicine.

The simplest way to address the distortion of the heart is through a surface display. This method can be thought of as viewing the heart as if it were held up in front of the observer. Since only one side of the heart can be seen at a time, the heart can be rotated about its long axis to produce a cine display of the undistorted myocardium at all angles. Two methods of surface display of myocardial data have been reported. In one technique, the myocardium is viewed as a shining surface with an external, computer-simulated light source illuminating the heart to enhance the three-dimensional effect (*32*). While the visual appearance is pleasing, the information about the regional distribution of radioactivity in the myocardium is lost. Typically, a threshold will be set: above a certain value the myocardium will be present, below the value there will be a void. Thus, the resulting image is very dependent on the threshold chosen (*33*).

An alternative method that preserves the radioactivity information and eliminates uncertainties associated with a threshold is to render the surface in a color or gray scale indicating the activity in each region. Activity can be displayed on either the detected myocardial surface (Fig. 7, right images) (*24*) or it can be mapped onto a standard ellipsoid (*30, 34*). In the former case, the maximum activity in the wall is used to define a myocardial surface, thus treating the myocardium as an infinitely thin shell. This assumption appears to be justified since variations in radioactivity within the thickness of the wall cannot be detected because of the limited spatial resolution of the gamma camera. Although a reflecting light source cannot be employed, the three-dimensional effect is preserved through intensity weighting with depth and through the three-dimensional quality added by rotation.

Functional Imaging. Myocardial imaging is not limited to display of the regional distribution of radioactivity. Functional images of important biochemical and dynamic parameters can also be displayed. Recently, a monoexponential fitting procedure was applied to voxels in serial myocardial images obtained with carbon-11-labeled acetate to determine the rate of myocardial oxygen consumption in units of μmol/g/min (*35*). These functional images were then processed using the same three-dimensional display techniques previously

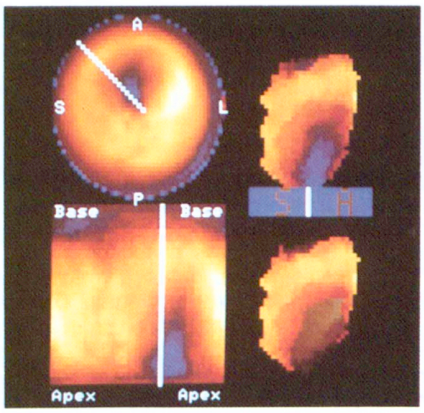

FIGURE 7
Rubidium-82 PET myocardial perfusion study in a patient with an antero-apical infarction. The bull's-eye display, with the apex at the center, is shown in the upper left image. A surface display with viewing of the heart from the side (apex oriented inferiorly) is shown in the upper right image. A Mercator display is shown on the lower left. A surface display after 50% thresholding, to allow view of the opposing wall through the defect, is shown on the lower right.

developed for myocardial images of radioactivity. Another investigator (*36*) developed a functional display derived from SPECT gated blood-pool studies in which the coloring of the blood-pool surface represents the degree of regional wall motion (Fig. 8).

Gated Blood-Pool Studies. The simplest approach to three-dimensional display of gated blood-pool studies, first described a decade ago, is a cine display of gated transaxial slices (*37*). The only significant technical requirements are the ability to acquire an 8- or 16-frame gated study at each angle as the SPECT camera rotates and the software to resort the data before reconstruction of the transaxial slices for each time frame. Display then consists simply of cine loops for each desired slice level (Fig. 9, upper images). This method, now being applied to gated CT and MR (*38*), has not become popular in nuclear medicine. The principal reason may be that the slice displays do not represent readily comprehensible three-dimensional information. The conventional two-dimensional method with acquisition and display at three or more angles is technically less demanding and the image information is much easier to assimilate.

The next logical step in the display of tomographic blood-pool studies was presentation of the gated slices in long- and short-axis orientations (*39–43*). While this approach has the advantages described above related to display in the coordinate system of the heart, interpretation of large numbers of beating slices is still cumbersome. This improvement also has not become popular, especially in view of the relative ease of acquisition and interpretation of planar studies.

The third important step in development of three-dimensional displays of gated blood-pool images was development of surface rendering techniques (*24, 36, 44*). Here, the margin of the cardiac blood pool is considered to be a surface. Following detection of this boundary by simple thresholding or more elaborate methods, standard surface rendering techniques are applied to produce rotating, three-dimensional images. This display method has achieved a degree of popularity, largely because of the availability of commercial software. While the technique is relatively easy to implement, there are two major problems. First, the boundary of the blood pool must be accurately determined. When thresholding is employed, the ventricles can be made to look either too small or very dilated by selection of a threshold that is, respectively, either too

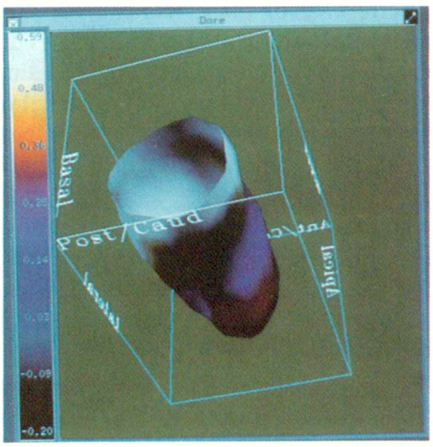

FIGURE 8
Image of the blood-pool surface from a gated SPECT blood-pool study. The color coding of the surface represents the degree of motion of the blood pool during the cardiac cycle. (Illustration courtesy of Tracy L. Faber, PhD.)

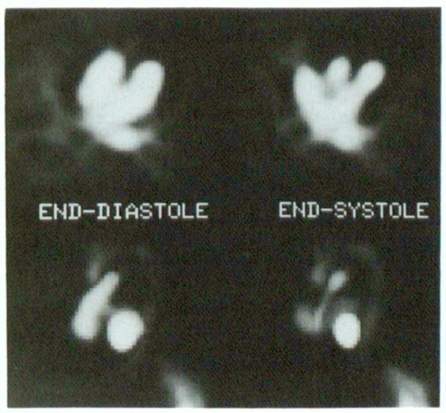

FIGURE 9
The upper images show end-diastolic and end-systolic transaxial slices at the mid-ventricular level from a tomographic gated blood-pool study of patient with anterior myocardial infarction. The lower images show the same study in the left anterior oblique orientation rendered with maximum activity projection.

high or too low (*6*). The second difficulty involves the partial volume effect. A very small ventricle at end-systole may actually seem to disappear because the blood-pool counts will drop due to volume averaging, causing the activity to fall below the fixed boundary threshold. More elaborate edge detection algorithms substantially reduce both these problems.

Recently, the maximum activity projection method of rendering has been applied to gated blood-pool studies employing labeled red blood cells in both SPECT and PET imaging (*7*). In this rendering technique, the problems associated with detection of the blood-pool boundary do not arise because boundary detection is not performed prior to display. Although the true surface is not displayed, the rotating cine presentation shows the blood pool boundary in a manner similar to that of planar gated imaging, with the advantages that many viewing angles are available and that contrast is enhanced (Fig. 9, lower images). While artifacts due to the partial volume effect can still arise, they are less of a problem with depth-weighted maximum activity because no thresholding is employed.

With all the techniques described above, digital "cardiac surgery" can be performed. It is relatively easy to digitally remove activity within any desired chamber and display the resulting data. For example, the right atrium can be digitally removed, leaving the right ventricle to be viewed or quantified without the overlapping atrium. In the right lateral position, the true anterior wall of the left ventricle can be seen after digital removal of the overlapping right ventricle.

Imaging of Other Organs

When imaging is performed to detect areas of decreased uptake, the volume rendering technique of maximum activity projection should not be utilized. For example, in renal cortical imaging, scintigraphy is performed to identify areas of decreased uptake caused by renal scarring. Such defects would be obscured by maximum activity projection. Because these scars are frequently located on the surface of the kidney, it is more appropriate to use one of the surface display techniques. Examples of normal and abnormal kidneys using a thresholded surface display are shown in Figure 10. If surface displays are employed, it is useful to be able to interactively manipulate cut planes through the rendered image to visualize interior organ structure (*45*).

The brain provides a greater challenge for three-dimensional display, because areas of both increased and decreased uptake are of interest to the viewer. Some investigators have applied bull's-eye displays to the brain, utilizing either counts from a thin rim along the outer margin of the brain which is between two fitted ellipses (*46*) or maximal counts radially (*47*). Thresholded surface displays (*48*), maximum activity projection, and volumetric compositing have also been applied to the brain, and investigators have mapped surface activity onto MR images, as described below. While all of these techniques are useful orientation aides during study interpretation, analysis directly from sagittal, coronal, and transverse slices may still be best for detection of abnormalities.

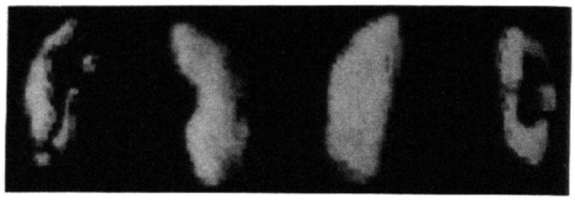

FIGURE 10
Surface display of the kidneys based on SPECT images obtained following administration of ^{99m}Tc-glucoheptonate. Rendering has been performed from both anterior and posterior views using the ANALYZE image processing package developed at the Mayo Clinic. The left kidney shows cortical defects from previous infections. (Illustration courtesy of John Keyes, Jr., MD.)

Clinical Applications Outside of Nuclear Medicine

CT of Craniofacial Deformities. An important clinical application of three-dimensional display has been developed by Vannier and colleagues at Washington University (*49*). They generate surface images of the face and skull from high-resolution CT scans. Plastic surgeons use these realistic images as an aid in planning and performing reconstructive surgery in patients with complex craniofacial deformities. This group has performed a careful investigation of the clinical utility of three-dimensional displays (*50, 51*). The investigators compared several display techniques in the evaluation of craniosynostosis, using a combination of radiologic and surgical findings as the gold standard. A comparison was performed of plain radiographs, CT slices, three-dimensional surface images with depth cues only, three-dimensional surface images with shading from simulated illumination, and three-dimensional volume-rendered images using a form of volumetric compositing (two of these techniques are illustrated in Fig. 4). Using ROC (receiver operating characteristic) analysis, the illuminated surface technique was found to give the best results, closely followed by volume rendering. Surface rendering with depth cues only performed the worst, and the standard techniques (radiographs and CT slices) were intermediate.

Other CT Applications. Reported applications of three-dimensional display in CT have included evaluation of shoulder pathology (*52*), hip fractures (*53*), imaging of the lung bronchial tree (*54*), and even imaging of an Egyptian mummy (*55*). Use of rendered images for quantitative measurements has been evaluated both for CT (*56, 57*) and MR images (*57*); results

uggest that measurement inaccuracies are present but elatively small. Several evaluations of three-dimenional displays have suggested that they are of use only n selected circumstances. Three-dimensional rendering was assessed in the evaluation of ankle fractures; while the rendered images were useful in surgical planning, investigators found that slices provided superior anatomic detail and information regarding the fractures (*58*). A retrospective review of the use of three-dimensional displays suggested that surface images are useful in evaluating the bony structure of the spine and other bone structures, but not in the investigation of soft-tissue alterations (*59*). A small controlled prospective study in the assessment of lung tumors showed that surface displays resulted in a slight gain in the assessment of arterial involvement compared to analysis of slices but with a dramatic loss of sensitivity in assessment of bronchial involvement (*60*). Thus, although most modern CT scanners have the ability to produce three-dimensional images, it is not always appropriate to rely on such displays for diagnostic purposes; one needs to be aware of how the images are generated and their resulting limitations.

MRI of the Heart. Three-dimensional surface displays have been used in the evaluation of congenital heart disease. Using gated MRI, Vannier et al. produced images clearly depicting the size and location of intracardiac defects (Fig. 11). These images were felt to be useful in the planning of reparative surgery (*61*, *62*).

MRI Cerebral Angiography. Cerebral angiograms can be produced using MR by applying a gradient-echo technique (*8*, *9*). Subsequent rendering using maximum activity projection produces images similar to that obtained from intra-arterial digital subtraction angiography. While this technique may not replace more invasive angiographic techniques, the authors found it useful in evaluating relationship of vessels to tumors and in the identification of intracranial aneurisms and large-vessel occlusive cerebrovascular disease.

MRI Seizure Evaluation. In the surgical treatment of epilepsy, correlation between electrode location and brain gyri is useful in planning the surgical resection. Investigators at the Mayo clinic report use of surface rendering to map electrode location onto surface images of the brain produced from MR images (*63*). Volume rendering has also been used to create images of the brain from MRI data (*64*).

Radiation Therapy Planning. Optimal beam planning in radiation therapy involves maximizing the delivered dose to tumor while minimizing exposure of surrounding tissue. Three-dimensional displays are being investigated as an aid to therapy planning, since they allow viewing of both projected beam outlines and isodose surfaces (Fig. 12) (*65*).

Combined Modalities

Brain Image Registration. Investigators at the University of Chicago have developed techniques for aligning PET and MR images, with subsequent merging of the two data sets into a three-dimensional display (*66*). Following alignment, images of the brain were produced from the MRI data utilizing volume rendering. An outer rim of the brain was defined on the PET data, and this information was then used to color the volume-rendered images (Fig. 13). While preliminary results were encouraging, the authors noted that the process was time-consuming and operator-dependent.

Cardiac Image Registration. To correlate anatomic and functional information, investigators have combined angiography and scintigraphic perfusion data into a single image. Early attempts displayed standard coronary anatomy using a normal set of coronary arteries superimposed upon a thresholded surface display (*67*). More recent work has employed patient-specific arter-

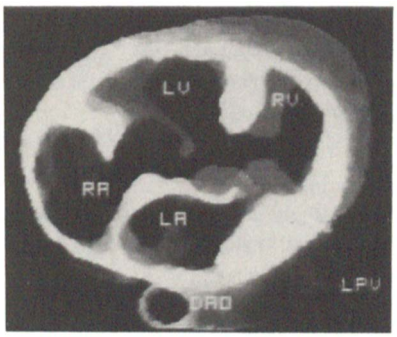

FIGURE 11
Surface rendering was performed on MR images of the heart from a patient with levo-transposition of the great vessels and a ventriculoseptal defect (VSD). From this caudocranial perspective, the four main cardiac chambers (RA, RV, LA, and LV) are visible. The VSD is visable, as are the left pulmonary vein (LPV) and descending aorta (DAO). (Illustration courtesy of M. Vannier, MD.)

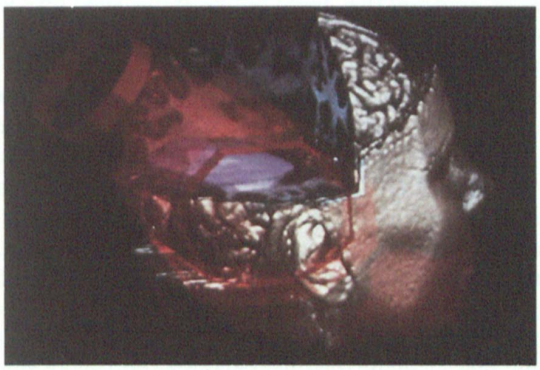

FIGURE 12
Volume rendering of an MR scan of a patient with a brain tumor. A polygonally defined target volume (purple) and treatment beams (red) are shown. A portion of the volume has been cut away and the raw MR values have been mapped onto the cutting planes. (Illustration copyright 1990 UNC/CH, M. Levoy and V. Interante, reprinted from Ref. 65 with permission.)

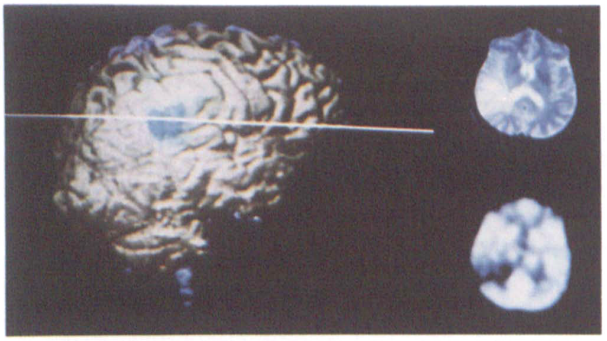

FIGURE 13
Preoperative images of a 48-yr-old man with a right parietal glioma. Multimodality display (left) shows the hypometabolic lesion superimposed on an MR brain surface image. The two panels at the right show an MR image and a PET image at the level marked by the line-cursor in the left panel. (Illustration courtesy of David N. Levin, MD, PhD. Reprinted from Ref. 66 with permission.)

iographic data (*34*, *68*). Following reconstruction of the coronary artery tree in three dimensions from bi-plane cine angiography, the arterial tree is mapped onto an ellipsoid that contains color-coded perfusion information from the scintigraphic study.

CONCLUSION

Tomographic imaging in radiology has allowed more accurate visualization of organ structures and enhanced our ability to detect small lesions. At the same time, image interpretation has become more complex; the viewer must deal with increasing numbers of images and be able to build up a mental picture of whole organs from a display of many slices. Three-dimensional displays have the potential to aid in image interpretation by providing an overview of the study; contiguity of structures across slices is enhanced and details may be apparent that could not be appreciated on slice displays. While increased diagnostic accuracy has been demonstrated in nuclear medicine only for the bull's-eye thallium display, physicians at several clinical sites who use three-dimensional volume rendering have reported increased speed and confidence in interpretation of clinical SPECT studies. Slice data should always be viewed along with the rendered images, however, until further investigations regarding the diagnostic value of these displays have been performed. Finally, three-dimensional displays may aid in conveying information to the referring physician, and ongoing research suggests that it may facilitate treatment planning and allow more accurate correlation of results obtained from different imaging modalities.

ACKNOWLEDGMENTS

This work was supported in part by National Heart, Lung, and Blood Institute grant HL42884 and by a grant from Siemens Medical Systems, Inc., Hoffman Estates, Illinois. W also thank Michael W. Vannier, MD for his comments durir preparation of this manuscript.

REFERENCES

1. Levoy M. Tutorial on volume visualization algorithms: introduction. In: *First conference on visualization in biomedica computing.* Atlanta, GA: University of North Carolina 1990:6–11.
2. Goris ML, Boudier S, Briandet PA. Interrogation and display of single photon emission tomography data as inherently volume data. *Am J Physiol Imaging* 1986;1:168–180.
3. Silverstein EA, Speis SM, Zimmer AM, Spies WG. Three-dimensional visualization of SPECT image data by presentation as stereo pairs. *J Nucl Med* 1988;29:810.
4. Chen H, Sedat JW, Agard DA. Manipulation, display, and analysis of three-dimensional biological images. In: Pawley J, ed. *The handbook of biological confocal microscopy.* Madison, WI: IMR Press; 1989:127–135.
5. Wallis JW, Miller TR. Volume rendering in three-dimensional display of SPECT images. *J Nucl Med* 1990;31:1421–1430.
6. Wallis JW, Miller TR, Lerner CA, Kleerup EC. Three-dimensional display in nuclear medicine. *IEEE Trans Med Imaging* 1989;8:297–303.
7. Miller TR, Wallis JW, Sampathkumaran KS. Three-dimensional display of gated cardiac blood-pool studies. *J Nucl Med* 1989;30:2036–2041.
8. Keller PJ, Drayer BP, Fram EK, Williams KD, Dumoulin CL, Souza SP. MR angiography with two-dimensional acquisition and three-dimensional display. Work in progress. *Radiology* 1989;173:527–532.
9. Masaryk TJ, Modic MT, Ross JS, et al. Intracranial circulation: preliminary clinical results with three-dimensional (volume) MR angiography. *Radiology* 1989;171:793–799.
10. Levoy M. Volume Rendering: Display of surfaces from volume rendered data. *IEEE Computer Graphics and Applications* 1988;29–37.
11. Drebin RA. Volume Rendering. *Comp Graphics* 1988;22:65–74.
12. Beck EG. Stereoscopic radiography as diagnostic aid in pulmonary tuberculosis. (Reprint of 1910 article). *AJR* 1981;137:890–891.
13. Kelsey CA, Moseley RDJ, Mettler FAJ, Briscoe DE. Cost-effectiveness of stereoscopic radiographs in detection of lung nodules. *Radiology* 1982;142:611–613.
14. Pratt AG, Kier EL, Rothman SG, Allen WE3. Polarized projection of stereo cerebral angiograms for audience viewing. *Am J Roentgenol* 1977;128:231–233.
15. Takahashi M, Ozawa Y. Routine biplane cerebral angiography with stereoscopic magnification. *Radiology* 1980;136:113–117.
16. Takahashi M, Bussaka H, Miyawaki M, Higashida Y. Stereoscopic technique in digital subtraction angiography. *Radiology* 1985;157:546.
17. Juni JE, Meyers LJ, Nicholas J, Brown G. Stereoscopic myocardial infarct imaging with Tc-99m-pyrophosphate [Abstract]. *J Nucl Med* 1985;26:P87.
18. Phong BT. Illumination for computer generated pictures. *Comm of the ACM* 1975;18:311–317.
19. Foley JD, Van Dam A. *Fundamentals of interactive computer graphics.* Reading, MA: Addison-Wesley; 1982:545.
20. Chen LS, Herman GT, Reynolds RA, Udupa JK. Surface shading in the cuberille environment. *IEEE Comput Graphics Appl* 1985;5:33–43.

21. Gargentini I, Walsh TR, Wu OL. Viewing transformations of voxel-based objects via linear octrees. *IEEE Comput Graph Appl* 1986;6:12–21.
22. Raya SP, Udupa JK. Shape-based interpolation of multidimensional objects. *IEEE Trans Med Imag* 1990;9:32–42.
23. Miller TR, Wallis JW, Grothe RA. Design of PET tomographs: the effect of slice spacing. *J Nucl Med* 1990;31:1732–1739.
24. Miller TR, Starren JB, Grothe RAJ. Three-dimensional display of positron emission tomography of the heart. *J Nucl Med* 1988;29:530–537.
25. Geist D, Vannier MW. PC-based 3-D reconstruction of medical images. *Comput Graphics* 1989;13:135–143.
26. Garcia EV, Van Train K, Maddahi J, et al. Quantification of rotational thallium-201 myocardial tomography. *J Nucl Med* 1985;26:17–26.
27. DePasquale EE, Nody AC, DePuey EG, et al. Quantitative rotational thallium-201 tomography for identifying and localizing coronary artery disease. *Circulation* 1988;77:316–327.
28. Van Train KF, Maddahi J, Berman DS, et al. Quantitative analysis of tomographic stress thallium-201 myocardial scintigrams: a multicenter trial. *J Nucl Med* 1990;31:1168–1179.
29. Kaul S, Boucher CA, Newell BA, et al. Determination of the quantitative thallium imaging variables that optimize detection of coronary artery disease. *J Am Coll Cardiol* 1986; 7:527–537.
30. Cooke CD, Garcia EV, Folks RD, Peifer JW, Ezquerra NF. Visualization of cardiovascular nuclear medicine tomographic perfusion studies. In: *First conference on visualization in biomedical computing*. Atlanta, GA: IEEE Computer Society Press; 1990:185–189.
31. Tamaki N, Ohtani H, Yonekur Y, et al. A new bull's-eye polar map display of thallium-201 SPECT imaging for quantitative measurement of perfusion defects. *J Nucl Med* 1990;31:808.
32. Nowak DJ. Three dimensional surface display of nuclear medicine images. *J Nucl Med* 1988;29:967.
33. Eisner RL, Aaron A, Nowak D, Dunn D, Patterson RE. Quantitation of thallium-201 SPECT: Comparison of the quantitative bull's-eye display and 3-D surface images. *J Nucl Med* 1988;29:757.
34. DePuey EG, Garcia EV, Ezquerra NF. Three-dimensional techniques and artificial intelligence in thallium-201 cardiac imaging. *Am J Roentgenol* 1989;152:1161–1168.
35. Miller TR, Wallis JW, Geltman EM, Bergmann SR. Three-dimensional functional images of myocardial oxygen consumption from positron tomography. *J Nucl Med* 1990;31: 2064–2068.
36. Faber TL, Stokely EM, Templeton GH, Akers MS, Parkey RW, Corbett JR. Quantification of three-dimensional left ventricular segmental wall motion and volumes from gated tomographic radionuclide ventriculograms. *J Nucl Med* 1989;30:638–649.
37. Moore ML, Murphy PH, Burdine JA. ECG-gated emission computed tomography of the cardiac blood pool. *Radiology* 1980;134:233–235.
38. Caputo GR, Higgins CB. Advances in cardiac imaging modalities: fast computed tomography, magnetic resonance imaging, and positron emission tomography. *Invest Radiol* 1990;25:838–854.
39. Tamaki N, Mukai T, Ishii Y, et al. Multiaxial tomography of heart chambers by gated blood-pool emission computed tomography using a rotating gamma camera. *Radiology* 1983;147:547–554.
40. Corbett JR, Jansen DE, Lewis SL, et al. Tomographic gated blood-pool radionuclide ventriculography: analysis of wall motion and left ventricular volumes in patients with coronary artery disease. *J Am Coll Cardiol* 1985;6:349–358.
41. Gill JB, Moore RH, Tamaki N, et al. Multigated blood-pool tomography: new method for the assessment of left ventricular function. *J Nucl Med* 1986;26:1916–1924.
42. Fischman AJ, Moore RH, Gill JB, Strauss HW. Gated blood-pool tomography: a technology whose time has come. *Semin Nucl Med* 1989;19:13–21.
43. Underwood SR, Walton S, Ell PJ, Jarritt PH, Emanuel RW, Swanton RH. Gated blood-pool emission tomography: a new technique for the investigation of cardiac structure and function. *Eur J Nucl Med* 1985;10:332–337.
44. Gibson CJ. Real time 3D display of gated blood pool tomograms. *Phys Med Biol* 1988;33:569–581.
45. Gibson CJ. A new method for the three-dimensional display of tomographic images. *Phys Med Biol* 1983;28:1153–1157.
46. Links JM, Loats HL, Holcomb HH, Loats SE, Stumpf MJ, Wagner HN. Cortical circumferential profiling: an objective approach to cortical quantification in emission tomography. *J Nucl Med* 1989;30:816.
47. Maurer AH, Siegel JA, Comerota AJ, Morgan WA, Johnson MH. SPECT quantification of cerebral ischemia before and after carotid endarterectomy. *J Nucl Med* 1990;31:1412–1420.
48. Webb S, Ott RJ, Flower MA, McCready VR, Meller S. Three-dimensional display of data obtained by single photon emission computed tomography. *Br J Radiol* 1987;60:557–562.
49. Vannier MW, Marsh JL, Warren JO. Three-dimensional CT reconstruction images for craniofacial surgical planning and evaluation. *Radiology* 1984;150:179–184.
50. Vannier MW, Hildebolt CF, Marsh JL, et al. Craniosynostosis: diagnostic value of three-dimensional CT reconstruction. *Radiology* 1989;173:669–673.
51. Pilgram TK, Vannier MW, Hildebolt CF, et al. Craniosynostosis: image quality, confidence, and correctness in diagnosis. *Radiology* 1989;173:675–679.
52. Kulhman JE, Fishman EK, Ney DR, Magid D. Two- and three-dimensional imaging of the painful shoulder. *Orthop Rev* 1989;18:1201–1208.
53. Robertson DD, Walker PS, Fishman EK, et al. The application of advanced CT imaging and computer graphics methods to reconstructive surgery of the hip. *Orthopedics* 1989;12:661–667.
54. Ney DR, Kuhlman JE, Hruban RH, Ren H, Hutchins GM, Fishman EK. Three-dimensional CT-volumetric reconstruction and display of the bronchial tree. *Invest Radiol* 1990; 25:736–742.
55. Magid D, Bryan BM, Drebin RA, Ney D, Fishman EK. Three-dimensional imaging of an Egyptian mummy. *Clin Imaging* 1989;13:239–240.
56. Hildebolt CF, Vannier MW, Knapp RH. Validation study of skull three-dimensional computerized tomography measurements. *Am J Phys Anthropol* 1990;82:283–294.
57. Smith DK, Berquist TH, An KN, Robb RA, Chao EY. Validation of three-dimensional reconstructions of knee anatomy: CT vs MR imaging. *J Comput Assist Tomogr* 1989;13: 294–301.
58. Magid D, Michelson JD, Ney DR, Fishman EK. Adult ankle fractures: comparison of plain films and interactive two- and three-dimensional CT scans. *AJR* 1990;154:1017–1023.
59. Pate D, Resnick D, Andre M, et al. Perspective: three-dimensional imaging of the musculoskeletal system. *AJR* 1986;147: 545–551.
60. Quint L, McShan D, Glazer G, Orringer M. Three-dimensional CT in central lung tumors. *AJR* 1988;150:460 (summarized in *Radiology Today* 1988; Aug. 18).
61. Vannier MW, Gutierrez FR, Laschinger JC, Gronemeyer S,

Canter CE, Knapp RH. Three-dimensional magnetic resonance imaging of congenital heart disease. *Radiographics* 1988;8:857–871.

62. Laschinger JC, Vannier MW, Gutierrez F, et al. Preoperative three-dimensional reconstruction of the heart and great vessels in patients with congenital heart disease. Technique and initial results. *J Thorac Cardiovasc Surg* 1988;96:464–473.
63. Jack CR, Marsh WR, Hirshcorn KA, et al. EEG scalp electrode projection onto three-dimensional surface rendered images of the brain *Radiology* 1990;176:413–418.
64. Rusinek H, Mourino MR, Firooznia H, Weinreb JC, Chase NE. Volumetric rendering of MR images. *Radiology* 1989; 171:269–272.
65. Levoy M, Fuchs H, Pizer S, et al. Volume rendering in radiation treatment planning. In: *First conference on visualization in biomedical computing.* Atlanta, GA: IEEE Computer Society Press; 1990:4–10.
66. Levin DN, Hu XP, Tan KK, et al. The brain: integrated three-dimensional display of MR and PET images. *Radiology* 1989;172:783–789.
67. Gibson CJ, Laird EE, Williams ED, Rajathurai A, Mittra B, Rankin D. New technique for showing the relation of tomographic myocardial perfusion images obtained with thallium-201 to the coronary arteries. *Br Heart J* 1985;54:367–374.
68. Cooke C, Jofre L, Klein L, et al. Three-dimensional reconstruction of arterial structure from biplane angiography. In: *IEEE technicon '87.* Institute of Electrical and Electronics Engineers; 1987:31–34.